

# Quality-Controlled Spectral Irradiance Data Processing for Photovoltaic Performance Modeling

Ivan Bevanda<sup>1</sup>, Petar Marić<sup>1</sup>, Zoran Injić<sup>1</sup>

<sup>1</sup>Faculty of Mechanical Engineering, Computing and Electrical Engineering University of Mostar, Bosnia and Herzegovina

<b>Abstract</b> Accurate spectral factor (SF) modeling for photovoltaic (PV) applications requires careful integration and analysis of spectral irradiance and broadband reference data. This study presents a robust methodology for preparing high-quality datasets suitable for developing spectral correction models. Specifically, the methodology encompasses (1) procedures for spectroradiometric extrapolation to reconstruct full-range solar irradiance from 280 to 4000 nm, and (2) protocols for validating the integrated spectroradiometer data against calibrated pyranometer measurements. The comparison between these measurement modalities is further examined as a function of the clearness index ( $K_t$ ) to assess the sensitivity of the spectral-broadband relationship under varying sky conditions, including overcast events. The approach is demonstrated using one year of high-frequency spectral and broadband irradiance data from the Lindenberg Meteorological Observatory in Germany (52.209275 °N, 14.120870 °E). The resulting quality-controlled dataset provides new insights into the influence of spectral variability on PV performance prediction. This reproducible framework enables systematic assessment of spectral-mismatch effects, supporting more accurate and reliable PV energy-yield modeling.	<b>Article history</b> Received: 1.12.2025. Revised: 24.12.2025. Accepted: 5.1.2026. <b>Keywords</b> Spectral Irradiance, Photovoltaic Performance, PV Modeling, Spectral Effects, Spectral Factor, Spectral Correction.
--	--

## 1 Introduction

The global transition to renewable energy is critical for mitigating climate change, with photovoltaic (PV) systems standing out as a key technology due to their ability to directly convert solar energy into electricity. However, accurately predicting PV performance under real-world conditions remains a complex challenge, as it is influenced by a multitude of environmental factors beyond simple broadband irradiance. While the effects of irradiance intensity and cell temperature are well-established, the impact of the solar spectrum's variability is often overlooked in both research and commercial simulation software like PVsyst and PV\*SOL [1].

This oversight stems from the historical dominance of crystalline silicon (c-Si), which is considered

relatively insensitive to spectral variations, leading to the widespread adoption of the standardized AM 1.5 spectrum for testing [2]. Nevertheless, spectral deviations caused by dynamic atmospheric conditions, geographical location, and season can induce performance variations of several percent in c-Si and significantly more in emerging thin-film and multi-junction technologies [3], [4], [5], [6], [7], [8]. Consequently, neglecting these effects can lead to non-negligible errors in energy yield predictions, sometimes exceeding 10% [9].

The core challenge in advancing spectral correction models lies in acquiring and processing high-quality, multi-source data. The spectral characterization of PV performance requires the synergistic integration of ground-based spectral irradiance measurements, broadband irradiance references, and key atmospheric parameters such as aerosol optical

**Contact** Ivan Bevanda, [ivan.bevanda@fsre.sum.ba](mailto:ivan.bevanda@fsre.sum.ba), Faculty of Mechanical Engineering, Computing and Electrical Engineering University of Mostar, Bosnia and Herzegovina

©2026 by the Author(s). Licensee IJISE by Faculty of Mechanical Engineering, Computing and Electrical Engineering, University of Mostar. This article is an open-access and distributed under the terms and conditions of the CC BY 4.0 (<https://creativecommons.org/licenses/by/4.0/>)

depth and precipitable water vapor. Crucially, the preparation of this data – including temporal synchronization, spatial interpolation, rigorous quality control, and filtering to isolate spectral effects from other losses, such as Angle-of-Incidence (AOI) – is paramount for developing robust mathematical correction models.

This paper presents a targeted methodology for the rigorous processing of spectral irradiance data acquired via a spectroradiometer, with a focus on extrapolation procedures to achieve comprehensive wavelength coverage from 280 nm to 4000 nm. A core aspect of the approach is the direct comparison of spectrally-derived irradiance values against calibrated pyranometer measurements to validate the data quality and consistency. Additionally, the relationship between spectroradiometer and pyranometer readings is systematically analyzed under varying clearness index ( $K_t$ ) levels to assess the influence of overcast and other sky conditions on the spectral-broadband agreement. This framework equips researchers and practitioners with reproducible procedures for evaluating the effects of spectral mismatch, ultimately supporting more accurate PV performance predictions across diverse environmental scenarios.

## 2 Methodology

### 2.1 Measurements

The measurements were conducted at the Lindenberg Meteorological Observatory (52.209275 °N, 14.120870 °E), Germany, which features a temperate oceanic climate (Cfb according to the Köppen-Geiger classification [10]). Both the spectroradiometer and the pyranometer were mounted horizontally on an unobstructed platform to ensure optimal exposure to solar radiation.

The spectral irradiance measurements were performed using a PSR spectroradiometer (PMOD/WRC) [11] which covers the spectral range from 300 to 1020 nm, with a wavelength accuracy of  $\pm 0.3$  nm and a spectral resolution of 1.5-5 nm (FWHM). The instrument employs a thermally stabilized CCD detector and integrating sphere input optics to ensure high measurement precision across

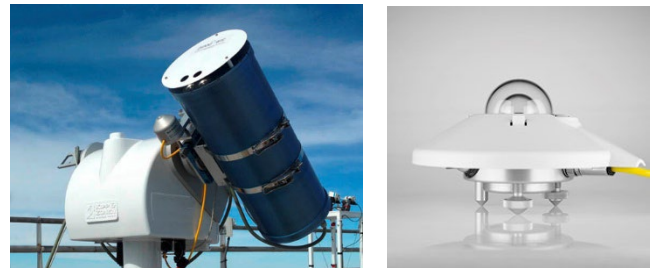


Figure 1 Spectroradiometer (left) and pyranometer (right)

the solar spectrum. Broadband global horizontal irradiance (GHI) was measured simultaneously using a Kipp & Zonen CMP22 pyranometer, classified as the highest-accuracy class (Spectrally Flat Class A) according to ISO 9060:2018. The CMP22 features a thermopile detector with quartz domes that provide exceptional spectral flatness across the solar spectrum, minimal temperature dependence, and low zero offsets [12]. Figure 1 shows the spectroradiometer and pyranometer used in this measurement campaign.

### 2.2 Extrapolation

The spectroradiometer used in this study measures solar spectral irradiance from 303 nm to 1020 nm. To calculate parameters that require the full solar spectrum (e.g., 280-4000 nm), such as the broadband irradiance or the spectral factor for PV devices, it was necessary to extrapolate the measured data into the unmeasured ultraviolet (UV, 280-303 nm) and near-infrared to mid-infrared (NIR-MIR, 1020-4000 nm) regions.

This work utilized two distinct extrapolation methods, based on the techniques established in [13,14], which have also been employed in later literature [15-17]. The core principle of both methods is to scale the standard reference spectrum AM1.5G to the unmeasured regions using the ratio between the measured and reference spectra in an adjacent, representative wavelength band. For the NIR-MIR extrapolation, the methodology of Martin and Ruiz was adopted. This approach is based on the premise that atmospheric extinction processes in the 700-1100 nm range are representative of those occurring in the longer-wavelength region beyond 1020 nm, which is dominated by absorption from water vapour and other uniformly mixed gases. The procedure is as follows: for each measured spectrum,

the ratio between the integrated irradiance  $E_{meas}(\lambda)$  of the measured spectrum and that of the standard reference spectrum,  $E_{ref}(\lambda)$ , in the 700-1100 nm band is calculated:

$$R_{NIR} = \frac{\int_{700}^{1100} E_{meas}(\lambda) d\lambda}{\int_{700}^{1100} E_{ref}(\lambda) d\lambda} \quad \text{Eq 1}$$

The extrapolated spectral irradiance for the 1020-4000 nm range,  $E_{extrap,NIR}(\lambda)$ , is then obtained by scaling the reference spectrum in this region by the factor  $R_{NIR}$ :

$$E_{extrap,NIR}(\lambda) = R_{NIR} \cdot E_{ref}(\lambda) \quad \text{Eq 2}$$

The extrapolation for the UV region followed the work of Neves et al. The same ratio-based method was applied, using the 303-340 nm band as the representative range for scaling, since it is adjacent to the unmeasured UV region and is subject to similar atmospheric influences from Rayleigh scattering and absorption by ozone ( $O_3$ ) and molecular oxygen ( $O_2$ ).

The final, complete spectrum  $E_{total}(\lambda)$  from 280 to 4000 nm is constructed by combining the three segments:

- The extrapolated UV part (280-303 nm)
- The directly measured part (303-1020 nm)
- The extrapolated NIR-MIR part (1020-4000 nm)

An example is shown in Figure 2 for three different measurements corresponding to three distinct levels of global horizontal irradiance. This method provides a physically consistent and practical approach to reconstructing the full solar spectrum, which is essential for accurate PV performance modeling and other spectral analyses. To further validate the physical consistency of the extrapolated spectra, the spectral factor (SF) - equivalent to the spectral mismatch factor - was calculated for nine different PV technologies. The SF for a given material was determined according to the following formula:

$$SF = \frac{\int E_{meas}(\lambda) SR(\lambda) d\lambda}{\int E_{ref}(\lambda) SR(\lambda) d\lambda} \cdot \frac{\int E_{ref}(\lambda) d\lambda}{\int E_{meas}(\lambda) d\lambda} \quad \text{Eq 3}$$

where  $SR(\lambda)$  is the spectral response of the device under test. The normalized spectral response for each of these nine materials is provided in Figure 3.

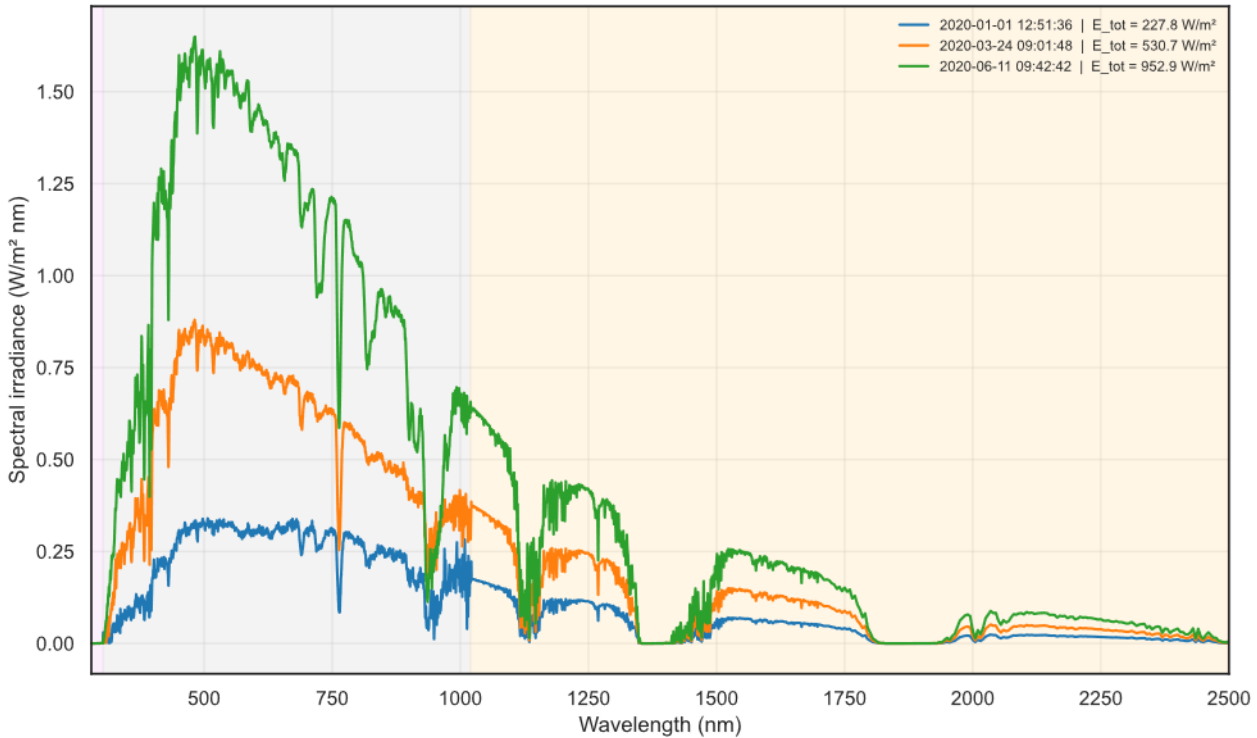


Figure 2 Reconstructed solar spectra with extrapolated UV and NIR regions for three distinct atmospheric conditions

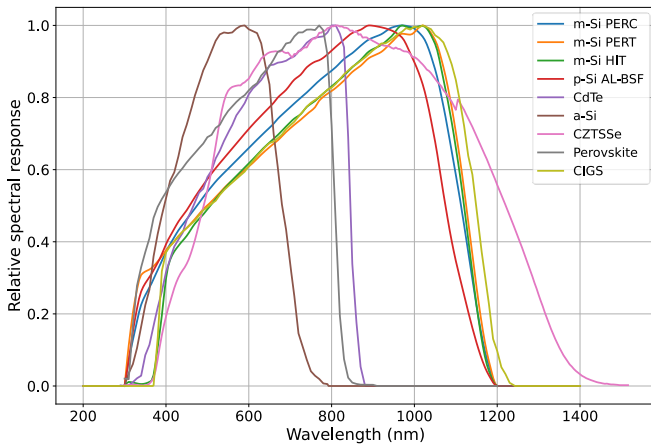


Figure 3 Normalized spectral responses of nine single-junction PV technologies

### 3 Results and discussion

#### 3.1 Overall model performance

The validation of the spectrally-derived global horizontal irradiance ( $GHI_{spec}$ ), calculated by integrating the reconstructed solar spectral irradiance across the complete wavelength range from 280 to 4000 nm, against the reference pyranometer measurements (GHI) demonstrates the high efficacy of the spectral extrapolation procedure. The analysis of 12,131 concurrent samples reveals an excellent agreement between the two datasets, as summarized in Table 1. The coefficient of determination ( $R^2$ ) of 0.924 indicates that the model explains the vast majority of the variance in the measured GHI. Furthermore, the slope of the regression line (0.926) is close to the ideal value of 1.0, and the intercept is  $18.139 \text{ W/m}^2$ . A small but consistent negative bias was observed, with a Mean Bias Error (MBE) of  $-2.05\%$  ( $-19.13 \text{ W/m}^2$ ), suggesting a slight overall underestimation by the spectral method. The Root Mean Square Error (RMSE) was found to be  $68.50 \text{ W/m}^2$ , corresponding to  $13.92\%$  of the mean measured GHI, which is a relatively high value and warrants further investigation into its underlying causes. This comparison is illustrated in Figure 4, where a scatter plot of spectrally-derived and pyranometer-measured GHI is presented, with a colour palette indicating the solar zenith angle values, providing insight into the angular dependence of the agreement.

Table 1 Statistical performance of the spectrally-derived  $GHI_{spec}$

Metric	Value	Value (%)
<b>Number of samples</b>	12,131	-
<b>MBE</b>	$-19.13 \text{ W/m}^2$	$-2.05$
<b>MAE</b>	$38.72 \text{ W/m}^2$	$7.74$
<b>RMSE</b>	$68.50 \text{ W/m}^2$	$13.92$
<b><math>R^2</math></b>	0.924	-
<b>Slope</b>	0.926	-

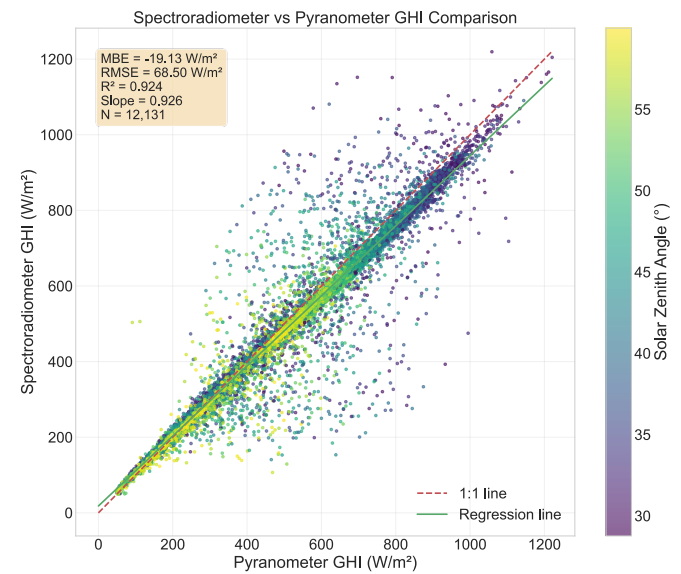


Figure 4 Scatterplot of spectrally derived and pyranometer-measured GHI

#### 3.2 Analysis of discrepancies and impact of transient clouds

The high RMSE value of  $13.92\%$ , compared to the relatively low MBE, is a key finding. It indicates that while the model is accurate on average, significant instantaneous discrepancies occur. We attribute these large, non-systematic errors primarily to transient cloud effects and the inherent challenge of temporally matching measurements from instruments with different sampling frequencies.

The pyranometer recorded data at one-minute intervals, while the spectroradiometer recorded measurements every five minutes. Although the GHI data were interpolated to match the spectroradiometer's timestamps, this procedure can introduce significant errors during periods of rapidly changing irradiance, such as the passage of cumulus

clouds. For instance, a spectroradiometer measurement captured during a sudden cloud passage would record a low spectral irradiance. However, if the linearly interpolated GHI value at that moment is derived from pyranometer measurements taken just before and just after the cloud's peak effect, it may not fully capture the irradiance dip, leading to a large positive difference ( $GHI_{spec} < GHI$ ). Conversely, if the cloud appears just after the spectroradiometer measurement but affects the pyranometer data used for interpolation, a large negative difference can occur. This temporal mismatch is a fundamental limitation when validating against a reference with a different sampling strategy and explains the high scatter (RMSE) observed in the results, as shown in Figure 5, where numerous sudden peaks in relative difference are evident.

Additionally, it is proposed to apply data filtering by removing values where  $K_t$  changes by more than 0.1 between consecutive measurements, and by excluding measurements for which the standard deviation of  $K_t$  over 15 consecutive samples exceeds 0.1, both of which should effectively mitigate transient cloud effects when perfect synchronization is not feasible. After applying the proposed data

filtering procedure and excluding records affected by transient clouds agreement between the  $GHI_{spec}$  and the reference pyranometer GHI improved considerably (Table 2). The analysis conducted on 7,326 samples yielded a coefficient of determination ( $R^2$ ) of 0.991, indicating an almost perfect linear relationship between the two datasets. The slope of the regression line (0.940) remained close to unity, while the intercept decreased to  $11.055 \text{ W/m}^2$ , further confirming the consistency of the spectral extrapolation method after temporal harmonization and filtering. The mean bias error (MBE) was significantly reduced from  $-19.13 \text{ W/m}^2$  ( $-2.05\%$ ) to  $-9.19 \text{ W/m}^2$  ( $-0.47\%$ ), effectively eliminating the systematic underestimation observed in the unfiltered dataset. More importantly, the root mean square error (RMSE) decreased from  $68.50 \text{ W/m}^2$  ( $13.92\%$ ) to  $22.78 \text{ W/m}^2$  ( $10.05\%$ ), demonstrating a substantial reduction in short-term discrepancies, as clearly evident in Figure 6, where the scatterplot of spectrally-derived and pyranometer-measured GHI for the filtered dataset is presented. The applied data filtering improved the overall agreement in the GHI comparison by reducing this scatter and removing samples affected by rapid short-term variability, but it did not eliminate the inherent systematic bias of the spectral model, which is intrinsic to the extrapolation procedure and is examined in detail in the following section. The reduced bias and strengthened correlation achieved after filtering therefore demonstrate that the spectrally-derived GHI reconstruction performs robustly under more stable atmospheric conditions, while simultaneously underscoring both the importance of synchronized sampling strategies in future measurement campaigns and the need to address the remaining systematic bias at the model level.

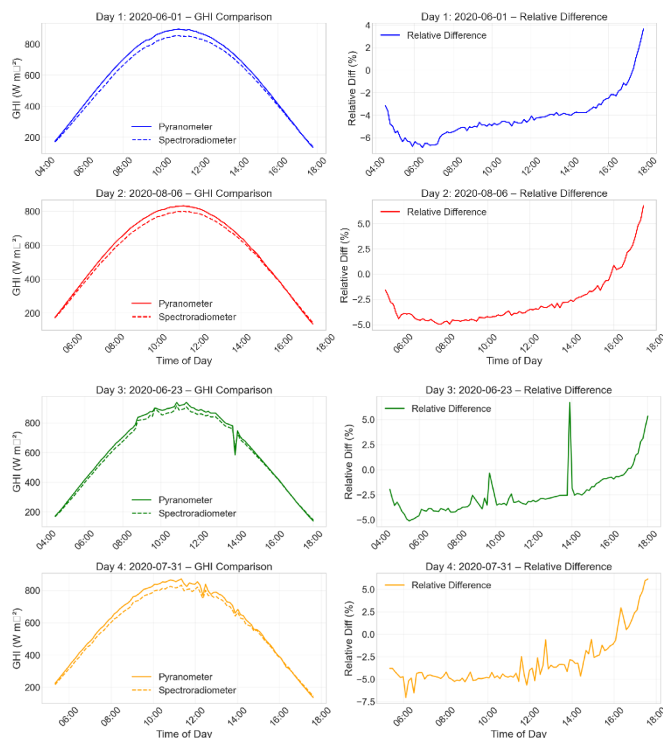


Figure 5 Scatterplot of spectrally derived and pyranometer-measured GHI

Table 2 Statistical performance of the filtered  $GHI_{spec}$

Metric	Value	Value (%)
<b>Number of samples</b>	7,326	-
<b>MBE</b>	$-9.19 \text{ W/m}^2$	$-0.47$
<b>MAE</b>	$17.07 \text{ W/m}^2$	$7.53$
<b>RMSE</b>	$22.78 \text{ W/m}^2$	$10.05$
<b><math>R^2</math></b>	0.991	-
<b>Slope</b>	0.940	-

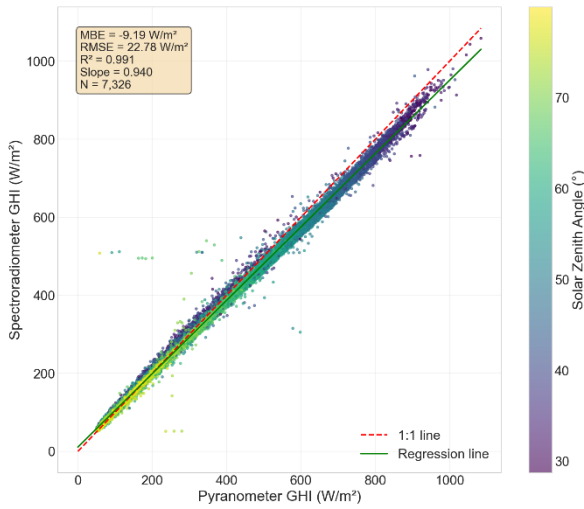


Figure 6 Scatterplot of spectrally derived and pyranometer-measured GHI for data filtered to avoid transient periods

### 3.3 Performance under different sky conditions

The further analysis reveals a systematic bias in the spectrally-derived Global Horizontal Irradiance ( $GHI_{spec}$ ) that is strongly dependent on the clearness index ( $K_t$ ) and is not due to previous data filtering. A consistent overestimation is observed under overcast conditions (low  $K_t$ ), while a systematic underestimation begins at approximately  $K_t = 0.5$  and increases with clearer skies. This relationship is clearly illustrated in Figure 7, which plots the relative difference between the integrated spectroradiometer  $GHI_{spec}$  and the reference pyranometer GHI against the clearness index.

This systematic error has a profound and non-physical impact on the calculated spectral factors (SF) for all nine PV materials analyzed. As shown in Figure 8, the spectral factors for all technologies exhibit a strong positive correlation with the clearness index.

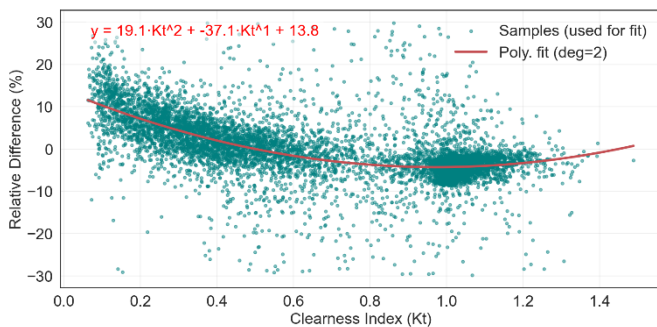


Figure 7 Relative GHI difference as a function of clearness index

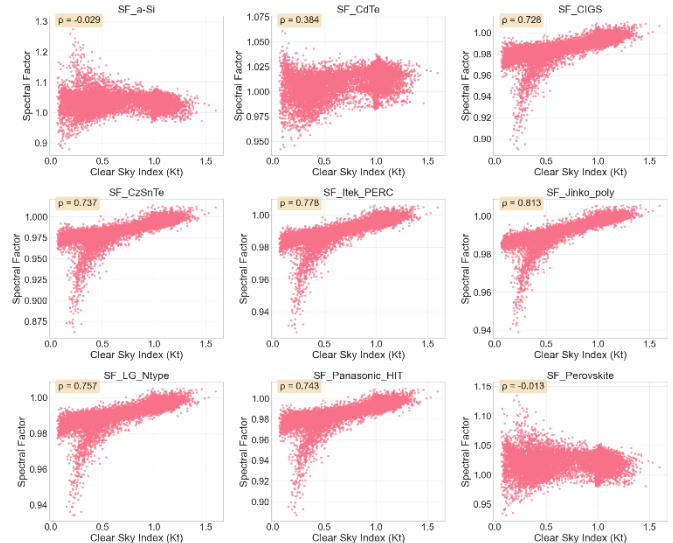


Figure 8 Spectral factors as a function of  $K_t$  for nine PV technologies

This finding is counter to established physical laws and expectations. Under overcast conditions, the combined effects of Mie scattering by cloud droplets and reduced Rayleigh scattering yield a diffuse spectrum enriched with shorter wavelengths. This means that the relative spectral content of solar radiation shifts towards the blue part of the spectrum (higher-energy photons), which should typically result in higher spectral factors for most PV materials under overcast skies than under clear skies. Therefore, a strong negative correlation is physically expected.

The observed positive correlation is a direct consequence of the systematic error introduced by the spectral extrapolation procedure. The overestimation of total GHI at low  $K_t$  and the underestimation at high  $K_t$  distort the underlying spectral distribution in the reconstructed spectra, leading to erroneous SF calculations that are inconsistent with atmospheric physics. To mitigate this significant source of error, a correction factor is proposed to adjust the integrated total irradiance value. The empirical relationship between the relative difference and the clearness index for this dataset is described by the second-order polynomial:

$$RD = 19,1K_t^2 - 37,1K_t + 13,8 \quad \text{Eq 4}$$

where RD is the relative difference (%), and  $K_t$  is the clearness index. This equation can be transformed

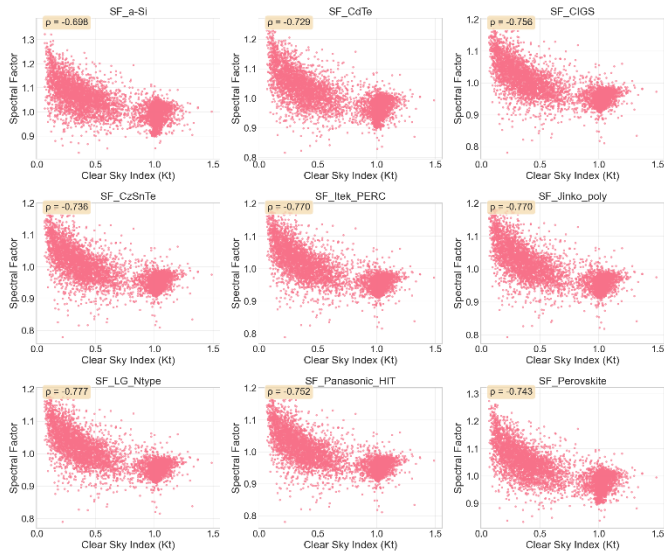


Figure 9 Corrected spectral factors as a function of  $K_t$  for nine PV technologies

into a direct correction factor for the integrated  $GHI_{spec}$ :

$$GHI_{corr} = \frac{GHI_{spec}}{\left(1 + \frac{19,1K_t^2 - 37,1K_t + 13,8}{100}\right)} \quad \text{Eq 5}$$

This correction systematically adjusts the spectrally-derived  $GHI_{spec}$  by reducing the overestimation at low  $K_t$  values and compensating for the underestimation at high  $K_t$  values, thereby producing spectral factors that exhibit the physically expected negative correlation with clearness index. The success of this correction is evident in Figure 9, where the corrected spectral factors for all nine PV materials now show the characteristic strong negative correlation consistent with atmospheric physics, in contrast to the non-physical positive correlation observed in the uncorrected data. However, the most straightforward and recommended approach, when both spectroradiometer and pyranometer measurements are available at the same location, is to use the directly measured pyranometer GHI for spectral factor calculations, thereby entirely bypassing the inaccuracies introduced by integrating and extrapolating the spectral data.

## 4 Conclusions

This study presents a rigorous methodology for processing high-quality spectral irradiance data suitable for photovoltaic performance modeling, with

particular focus on spectral extrapolation procedures and validation against calibrated broadband measurements. The key conclusions are:

- Overall accuracy of spectral extrapolation: The spectral extrapolation method demonstrates high overall accuracy for integrated broadband irradiance, with a strong linear relationship ( $R^2 = 0.924$ ) to reference pyranometer measurements under unfiltered conditions. This confirms that the procedure is well-suited to applications where precise prediction of the total available solar power is paramount. However, the high instantaneous errors (RMSE = 13.92%) are primarily attributable to transient cloud effects and temporal mismatches between the 5-minute spectroradiometer and 1-minute pyranometer sampling frequencies, rather than fundamental deficiencies in the extrapolation model itself.
- Impact of data filtering: The application of proposed data filtering criteria—removing values where the clearness index ( $K_t$ ) changes by more than 0.1 between consecutive measurements and excluding those with standard deviation exceeding 0.1 over 15 consecutive samples—substantially improved agreement under stable atmospheric conditions ( $R^2 = 0.991$ , RMSE = 10.05%). This filtering approach effectively eliminates transient artifacts and clarifies the underlying systematic behavior of the extrapolation procedure. However, the filtering did not eliminate the inherent systematic bias of the spectral model, which remains dependent on atmospheric conditions.
- Systematic bias as a function of sky conditions: A critical finding is the strong dependence of systematic bias on the clearness index. The spectrally-derived GHI exhibits overestimation under overcast conditions (low  $K_t$ ) and systematic underestimation under clear skies (high  $K_t$ ). This bias is independent of data filtering and is intrinsic to the integration and extrapolation procedure. The bias distorts the spectral distribution in reconstructed

spectra, leading to physically inconsistent spectral factor calculations that contradict established atmospheric physics—specifically, a non-physical positive rather than expected negative correlation with clearness index. In summary, while the extrapolation procedure is robust for predicting overall GHI and thus valuable for general energy-yield estimates, its direct application to high-precision spectral analysis is limited. The systematic biases identified herein must be corrected to ensure the physical validity of the derived spectral metrics, paving the way for more reliable spectrally resolved solar resource assessments.

- **Correction strategy and practical recommendations:** To address the systematic  $K_t$ -dependent bias, a second-order polynomial correction factor was derived and validated, demonstrating the recovery of physically consistent spectral factors. However, the most straightforward and recommended approach when both spectroradiometer and pyranometer measurements are available is to use the directly measured pyranometer GHI for spectral factor calculations, thereby entirely bypassing the inaccuracies introduced by spectral integration and extrapolation.
- **Future measurement campaigns:** For future high-temporal-resolution spectral studies, synchronizing the sampling frequencies of all instruments is strongly recommended. Where perfect synchronization is not feasible, the combined filtering and correction procedures presented herein provide an effective pathway to mitigate both transient artifacts and systematic biases.

In summary, while the spectral extrapolation procedure is robust for estimating total irradiance and general energy yield predictions, its direct application for high-precision spectral analysis requires careful consideration of systematic biases and appropriate corrections. This methodology provides researchers with reproducible, physics-informed procedures for preparing quality-controlled spectral datasets and for understanding

the limitations and proper applications of spectroradiometric data in PV modeling contexts.

**Conflicts of Interest:** The author(s) report there are no competing interests to declare;

## References

- [1] T. Betti, I. Bevanda, I. Marasović, and I. Zulim, "A new approach to comparing photovoltaic simulation software," *Energy Sources, Part A: Recovery, Utilization, and Environmental Effects*, vol. 45, no. 2, pp. 6290–6304, Jun. 2023, doi: 10.1080/15567036.2023.2215196.
- [2] G. S. Kinsey *et al.*, "Impact of measured spectrum variation on solar photovoltaic efficiencies worldwide," *Renewable Energy*, vol. 196, pp. 995–1016, Aug. 2022, doi: 10.1016/j.renene.2022.07.011.
- [3] G. S. Kinsey, "Solar cell efficiency divergence due to operating spectrum variation," *Solar Energy*, vol. 217, pp. 49–57, Mar. 2021, doi: 10.1016/j.solener.2021.01.024.
- [4] L. A. Conde, J. R. Angulo, M. Á. Sevillano-Bendezú, G. Nofuentes, J. A. Töfflinger, and J. De La Casa, "Spectral effects on the energy yield of various photovoltaic technologies in Lima (Peru)," *Energy*, vol. 223, p. 120034, May 2021, doi: 10.1016/j.energy.2021.120034.
- [5] D. Dirnberger, G. Blackburn, B. Müller, and C. Reise, "On the impact of solar spectral irradiance on the yield of different PV technologies," *Solar Energy Materials and Solar Cells*, vol. 132, pp. 431–442, Jan. 2015, doi: 10.1016/j.solmat.2014.09.034.
- [6] J. Polo, M. Alonso-Abella, J. A. Ruiz-Arias, and J. L. Balenzategui, "Worldwide analysis of spectral factors for seven photovoltaic technologies," *Solar Energy*, vol. 142, pp. 194–203, Jan. 2017, doi: 10.1016/j.solener.2016.12.024.
- [7] M. Alonso-Abella, F. Chenlo, G. Nofuentes, and M. Torres-Ramírez, "Analysis of spectral effects on the energy yield of different PV (photovoltaic) technologies: The case of four specific sites," *Energy*, vol. 67, pp. 435–443, Apr. 2014, doi: 10.1016/j.energy.2014.01.024.
- [8] I. Bevanda, P. Marić, A. Kristić, and T. Betti, "Assessing the Impact of Solar Spectral Variability on the Performance of Photovoltaic Technologies Across European Climates," *Energies*, vol. 18, no. 14, p. 3868, Jul. 2025, doi: 10.3390/en18143868.
- [9] M. Ruben Vogt *et al.*, "PV Module Energy Rating Standard IEC 61853-3 Intercomparison and Best Practice Guidelines for Implementation and Validation," *IEEE J. Photovoltaics*, vol. 12, no. 3, pp. 844–852, May 2022, doi: 10.1109/JPHOTOV.2021.3135258.
- [10] D. Cui, S. Liang, D. Wang, and Z. Liu, "A 1 km global dataset of historical (1979–2013) and future (2020–2100) Köppen–Geiger climate classification and bioclimatic variables," *Earth Syst. Sci. Data*, vol. 13, no. 11, pp. 5087–5114, Nov. 2021, doi: 10.5194/essd-13-5087-2021.
- [11] J. Gröbner and N. Kouremeti, "The Precision Solar Spectroradiometer (PSR) for direct solar irradiance measurements," *Solar Energy*, vol. 185, pp. 199–210, Jun. 2019, doi: 10.1016/j.solener.2019.04.060.
- [12] G. Sanchez, M. L. Cancillo, and A. Serrano, "An intercomparison of the thermal offset for different pyranometers," *JGR Atmospheres*, vol. 121, no. 13, pp. 7901–7912, Jul. 2016, doi: 10.1002/2016JD024815.
- [13] N. Martín and J. M. Ruiz, "A new method for the spectral characterisation of PV modules," *Prog. Photovolt: Res. Appl.*, vol. 7, no. 4, pp. 299–310, Jul. 1999, doi: 10.1002/(SICI)1099-159X(199907/08)7:4<299::AID-PIP260>3.0.CO;2-0.
- [14] G. Neves, W. Vilela, E. Pereira, M. Yamasoe, and G. Nofuentes, "Spectral impact on PV in low-latitude sites: The case of southeastern Brazil," *Renewable Energy*, vol. 164, pp. 1306–1319, Feb. 2021, doi: 10.1016/j.renene.2020.10.128.
- [15] G. Nofuentes, B. García-Domingo, J. V. Muñoz, and F. Chenlo, "Analysis of the dependence of the spectral factor of some PV technologies on the solar spectrum distribution," *Applied Energy*, vol. 113, pp. 302–309, Jan. 2014, doi: 10.1016/j.apenergy.2013.07.044.
- [16] J. A. Caballero, E. F. Fernandez, M. Theristis, F. Almonacid, and G. Nofuentes, "Spectral Corrections Based on Air Mass, Aerosol Optical Depth, and Precipitable Water for PV Performance Modeling," *IEEE J. Photovoltaics*, vol. 8, no. 2, pp. 552–558, Mar. 2018, doi: 10.1109/JPHOTOV.2017.2787019.
- [17] G. Nofuentes, J. De La Casa, E. M. Solís-Alemán, and E. F. Fernández, "Spectral impact on PV performance in mid-latitude sunny inland sites: Experimental vs. modelled results," *Energy*, vol. 141, pp. 1857–1868, Dec. 2017, doi: 10.1016/j.energy.2017.11.078.